Analyst

COMMUNICATION

View Article Online
View Journal | View Issue

Check for updates

Cite this: *Analyst*, 2017, **142**, 1676

Received 4th January 2017,
Accepted 21st April 2017

DOI: 10.1039/c7an00022g

rsc.li/analyst

Published on 27 April 2017. Downloaded by Wake Forest University on 20/06/2017 13:51:53.

Solid-state nanopore analysis of alcohol-soluble molecules†

Dhrubajyoti Basu Roy‡[a] and Adam R. Hall *[a,b]

We report on a modified solid-state nanopore measurement scheme to probe alcohol-soluble proteins. Taking advantage of the intrinsic alcohol solubility of LiCl as an electrolyte, we show that the devices can be operated in azeotropic mixtures of ethanol and water. We first characterize nanopore conductivity across a range of ethanol content as a function of both nanopore diameter and salt concentration, showing ionic response that can be understood through established models. Then, as a demonstration of resistive-pulse sensing, we measure and interpret electrical translocations of zeins, a class of alcohol-soluble maize protein.

Introduction

Despite their presence in a wide range of organisms,[1,2] alcohol-soluble proteins are an understudied class of molecule. This is due chiefly to the relative lack of techniques that are able to investigate them; because most biomolecules are hydrophilic, most assessments are consequently designed to function only in water-based environments, thereby requiring denaturation of water-insoluble molecules for study. Accordingly, the roles and properties of these proteins have been investigated far less than their water-soluble counterparts. However, in recent years, a particular consequence of alcohol-soluble proteins has gained visibility with the rise in prevalence of Celiac's disease and gluten intolerance.[3] Here, grain storage proteins rich in proline and glutamine ('prolamins', collectively) that are only soluble in high-concentration alcohol solutions cannot be fully degraded by enzymes in the gut due to their hydrophobicity. The resulting peptide chains are subsequently transported through the gut lumen where they cause an immune reaction. The ensuing inflammation further permeabilizes the lumen, thus enabling additional invasion and amplification of the response. Prolamin detection and assessment in particular could therefore enhance food safety, help elucidate the mechanisms of disease, and contribute to the development of treatments. Beyond this specific case, however, there are also a range of other proteins that exhibit new properties in alcohol, including improved stability and activity[4] or increased transmembrane transport,[5] as well as many synthetic nanoparticles that are soluble primarily in alcohol.[6–8] Therefore, new approaches to detecting molecules directly in alcohol solutions are needed.

Here, we accomplish this using solid-state (SS-) nanopores,[9,10] an emerging analytical platform for molecular detection. In the general approach, a thin membrane with a single, nanometer-scale opening stands between two basins of ionic solution. A trans-membrane applied voltage provides an electric field that both transports charged molecules through the pore and sets up a measurable ionic current. Interruptions to this current, also known as resistive pulses, mark translocation events and careful analysis of their shape and duration can be used to infer properties of individual passing molecules. This technology has been used to study a wide range analytes, including biomolecules like DNA,[11,12] RNA,[13,14] and proteins,[15–17] as well as synthetic nanoparticles[18–20] and other small molecules.[21]

SS-nanopore measurements, typically performed in electrolytic water solutions, have already been demonstrated in a range of alternative solvents. For example, glycerol–water mixtures[22] and two-phase systems[23] have each been used to alter the translocation speed of DNA. However, these changes in solution properties do not enable the study of non-traditional molecules like alcohol-soluble proteins. Similarly, ionic liquids have been used to achieve single nucleotide resolution measurements in small MoS_2 nanopores.[24] Here again, though, high fluid viscosity was the central enabling property.

[a]*Virginia Tech-Wake Forest School of Biomedical Engin and Sciences, Wake Forest University School of Medicine, Winston-Salem, NC 27101, USA*
[b]*Comprehensive Cancer Center, Wake Forest University School of Medicine, Winston-Salem, NC 27101, USA. E-mail: arhall@wakehealth.edu*

†Electronic supplementary information (ESI) available: Materials and methods, conductance noise comparisons for different ethanol compositions, results of a conductance model considering only fluid electrical permittivity differences, example current traces, event dwell time histograms, an additional protein gel, and analyses from an additional pore. See DOI: 10.1039/c7an00022g

‡Current address: Department of Molecular Medicine, Beckman Research Institute, City of Hope, Duarte, CA 91010.

This journal is © The Royal Society of Chemistry 2017

Published on 27 April 2017. Downloaded by Wake Forest University on 20/06/2017 13:51:53.

While hydrophobic ionic liquids[25] could in principle support the study of non-traditional molecules, this has not been demonstrated. Furthermore, it is not obvious that they would be amenable to use in the system, especially in terms of wetting the inside of a nanometer-scale pore.

We therefore implemented SS-nanopores directly with alcohol-based solvents. The chief hurdle to this approach is that the electrolytes most often used with the platform (KCl, NaCl) have extremely low solubilities in alcohol, precluding the central metric of the approach. However, due to the more covalent nature of the LiCl bond, it in particular is known[26] to have exceptional solubility in a range of alcohols that include ethanol and methanol. This offers a potential pathway to carry out conventional measurements with the system using solutions that can support alcohol-soluble proteins. Here, we use this simple observation to expand the functionality of SS-nanopores to high concentration azeotropic mixtures of ethanol and water.

Results & discussion

SS-nanopore ionic conductance in high-percentage alcohol

To develop the versatility of SS-nanopores as a measurement platform in high-concentration alcohol solutions, their ability to support predictable ionic flux first had to be established, since this is essential to resistive pulse sensing in general. Consequently, we first investigated trans-pore ionic current in azeotropic mixtures of ethanol and water. Fig. 1a shows a schematic of the measurement setup, which is identical to other conventional investigations with the system.[27] For these measurements, 3 M LiCl was employed as an electrolyte. This particular concentration was chosen to be near the maximum solubility of the salt in pure ethanol[28] (*i.e.* the lowest solubility expected for our array of measurements). Even upon varying the concentration of ethanol relative to water in the mixture, we observed that the SS-nanopore exhibited robust, linear current–voltage characteristics ($R^2 > 0.99$) over the entire investigated range (Fig. 1a, top inset) with a sharp decrease in measured conductance as ethanol content was increased. We also observed only minor differences in the SS-nanopore conductance noise spectra between solutions either with or without ethanol (c.f. ESI Fig. S1†).

Expanding this same measurement across a series of individual nanopores of increasing size, we found a consistent non-linear relationship between pore diameter and conductance (Fig. 1b) across all ethanol conditions, similar to what has been measured in water-based solutions elsewhere.[29] Accounting for the access regions, the measured conductance of a SS-nanopore can be expressed[30] as

$$G = \sigma_{\text{bulk}}\left[\frac{4L_{\text{eff}}}{\pi d^2} + \frac{1}{d}\right]^{-1}, \quad (1a)$$

where σ_{bulk} is the bulk conductivity of the solution, d is pore diameter, and L_{eff} is effective thickness of the membrane at the pore. Following a convention that accounts for the shape of the pore cross-section,[30] we used 10 nm for L_{eff} and then fit to the 0% ethanol data by varying σ_{bulk} (Fig. 1b, black dashed line). From this, we obtained a value for the bulk conductance of LiCl in water of 16.5 S m^{-1}, very close to the literature value[28] of 17.2 S m^{-1}. Repeating the same fit procedure for the remaining ethanol mixtures (Fig. 1b, dashed lines), we found a strong reduction in the effective σ_{bulk} as ethanol content increased. Indeed, plotting the fit parameters across all conditions indicated an exponential decrease in the value (Fig. 1c, black), highlighting the strong dependence of ionic current-carrying capacity on mixture ratio.

For a more complete characterization of SS-nanopores with azeotropic solutions, we next explored the relation between ionic conductance and salt concentration. We began by measuring salt dependence using KCl in water (Fig. 2, open symbols) and observed a non-linear relationship that was nearly identical to previous extensive characterization by Smeets, *et al.*[27] To analyze this data, eqn (1a) must be

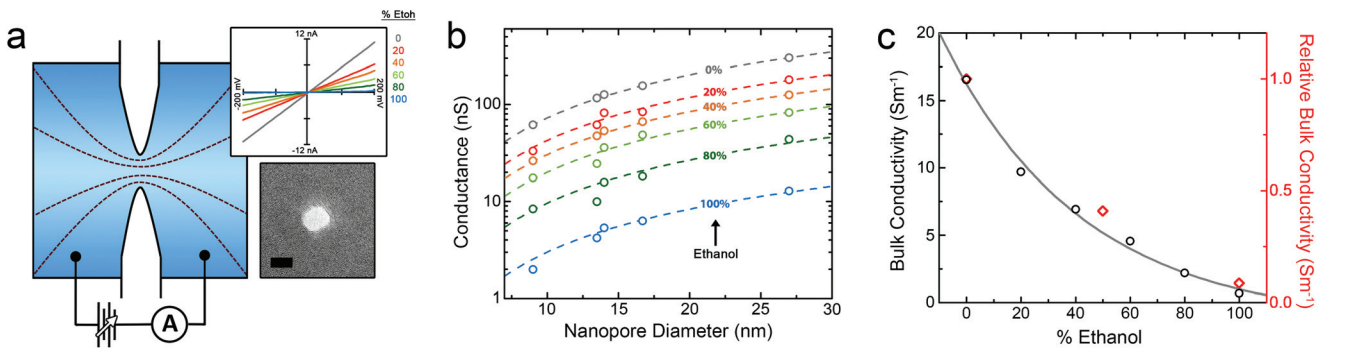

Fig. 1 (a) Schematic of the ethanol–water ionic flux measurement, where fluid (blue) ratio is varied. Dashed lines represent electric field. Top inset: Current–voltage characteristics of a typical SS-nanopore (diameter 6 nm) in ethanol–water mixtures containing 3 M LiCl. Ethanol percentages are 0% (grey), 20% (red), 40% (orange), 60% (light green), 80% (dark green), and 100% (blue). Bottom inset: transmission electron micrograph of a typical SS-nanopore, fabricated using the same technique. Scale bar is 10 nm. (b) SS-nanopore conductance *vs.* diameter as a function of ethanol content. Open symbols are experimental data and dashed lines are fits to eqn (1a) (see text for details). (c) Black symbols: apparent solution bulk conductivity (σ_{bulk}) derived from the fits in (b). Red symbols: change in σ_{bulk} derived from the analysis in Fig. 2, corresponding to right axis only.

Published on 27 April 2017. Downloaded by Wake Forest University on 20/06/2017 13:51:53.

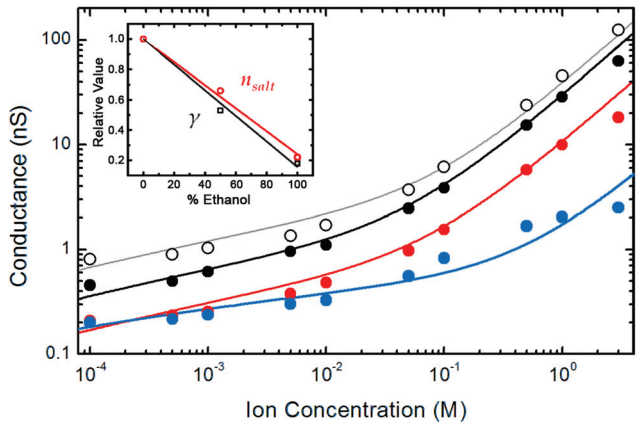

Fig. 2 SS-nanopore (pore diameter 6.8 nm) conductance as a function of ionic concentration under various conditions. Open black symbols are KCl in water; closed black symbols are LiCl in water; red symbols are LiCl in a 1 : 1 mixture of ethanol and water; and blue symbols are LiCl in absolute ethanol. Lines are fits to the experimental data using eqn (1b) and (2) (see text). Inset: Relative change in the values of n_{salt} and γ (*i.e.* multiplier of μ_{cat} and μ_{an}) required for LiCl fits.

expanded to account for the ionic dependence of solution bulk conductivity, σ_{bulk}, as[27]

$$G = \sigma_{bulk}\left[\frac{4L_{eff}}{\pi d^2} + \frac{1}{d}\right]^{-1} = \left((\mu_{cat} + \mu_{an})n_{salt}e + \mu_{cat}\frac{4S}{d}\right)\left[\frac{4L_{eff}}{\pi d^2} + \frac{1}{d}\right]^{-1}, \quad (1b)$$

where n_{salt} is the number density of ions (note that this can be expressed in terms of molarity using $n_{salt}/(A_n \times 1000)$, where A_n is Avagadro's number), e is the elementary charge, S is the surface charge density of the pore walls, and μ_{cat} and μ_{an} are electrophoretic mobilities of the cation and anion, respectively. Applying this model to our KCl data, we used values[28] of 7.35×10^{-8} m^2 V^{-1} s^{-1} for μ_{cat}, and 7.63×10^{-8} m^2 V^{-1} s^{-1} for μ_{an}, and again used 10 nm for L_{eff}. The salt dependent value of S was calculated using the combined expression[31]

$$S = \left(\frac{2\varepsilon\varepsilon_o k_B T\kappa}{e}\right) \times \sinh\left[\frac{1}{2}\ln\left(\frac{-S}{e\Gamma + S}\right) + \frac{1}{2}(pK - pH)\ln(10) - \frac{eS}{2k_B TC}\right] \quad (2)$$

where ε and ε_o are permittivities of the solution and of free space, respectively, k_BT is thermal energy, κ is the inverse of the Debye screening length ($\kappa^2 = 2e^2 n_{salt}/k_BT\varepsilon\varepsilon_o$), Γ is the density of chargeable surface sites, pK is the equilibrium constant, and C is Stern layer capacitance. Note that this expression incorporates the membrane zeta potential, as described elsewhere.[31] Since the silicon nitride used as the membrane material here will feature a native oxide layer at its surface, we then used values from ref. 27 for silicon dioxide and allowed d to vary as a free parameter. This yielded a best fit (Fig. 2, grey line) value of 6.8 nm, in good agreement with the target diameter from fabrication of 8 nm.

Subsequently replacing the electrolyte in the system with LiCl while retaining water as the solvent produced a qualitatively similar trend of conductance (Fig. 2, black closed symbols). We found that the quantitative differences could be well-described by simply substituting 3.9×10^{-8} m^2 V^{-1} s^{-1} as the value[28] of μ_{cat} for the new Li cation, but keeping all other variables (including d) the same (Fig. 2, black line). This demonstrated the robustness of the model for water-based solutions.

We next performed the same measurement in both a 1 : 1 mixture of water in ethanol (Fig. 2, red symbols) and in absolute ethanol (Fig. 2, blue symbols). For each of these, we observed downward shifts in nanopore conductance across the investigated salt concentration range relative to water. Examining the expressions above, the most obvious variable to adjust to account for the change in solution composition would be permittivity, ε, in eqn (2). However, substituting literature values[32] for either alternative fluid did not yield differences in the trend significant enough to explain the data (ESI Fig. S2†).

We therefore turned to two additional factors that could also be expected to play a role. First, the presence of ethanol can increase the association of Li^+ and Cl^- ions in solution, as has been demonstrated experimentally;[33] while remaining soluble, associated ions would not contribute to ionic transport, thereby reducing the measured ionic current. This could be represented in the model as an apparent reduction in n_{salt}. Second, the electrophoretic mobilities of ions that do dissociate could be diminished due to the solvation properties of the fluid. This effect would manifest as a change in μ_{cat} and μ_{an} in eqn (1b). For simplicity, we assume here that the change in μ_{cat} and μ_{an} is equivalent, *i.e.* that each is scaled by a common factor, γ. Returning to the data, we therefore allowed both n_{salt} and γ to vary as free parameters, with all other values kept constant. The resulting fits showed good correlation with the experiments (Fig. 2, red and blue lines). Interestingly, both of the free parameters themselves appeared to change monotonically with ethanol content, and each at a similar rate (Fig. 2, inset). Using the resulting n_{salt} and γ, the variation of effective σ_{bulk} could be determined, yielding relative values that agree well with our initial diameter-dependent measurements (Fig. 1c, red diamonds) and demonstrating the consistency of our data.

SS-nanopore detection of hydrophobic proteins

With a detailed description of LiCl ionic conductance using ethanol–water mixtures in SS-nanopores, we next focused on utilizing the platform to analyze alcohol-soluble proteins. For the initial demonstration, we chose as a standard molecule α-zein protein, the chief component of a class of alcohol-soluble maize prolamins that constitute the major storage protein group in the corn endosperm.[34] Zeins have been a subject of study in the food industry, and zein-based nanoparticles are attractive as potential drug-delivery vehicles due

 This journal is © The Royal Society of Chemistry 2017

Published on 27 April 2017. Downloaded by Wake Forest University on 20/06/2017 13:51:53.

to their biocompatibility and hydrophobicity.[35] Recently, it has also been suggested that, similar to the more familiar wheat-based gliadins, zeins could be linked with Celiac's disease,[36] making them a target of interest for immunogenic research.

α-zein consists predominantly of a 22 kDa protein that comprises[37] 9-10 anti-parallel α-helices joined by glutamine-rich loops and forms a quasi-cylindrical structure about 16 nm in length (Fig. 3a). While small, this is within the range of sizes that can be probed by SS-nanopores. For our experiments, pre-purified and lyophilized zein protein was resuspended in solution under heat and gentle mixing (see ESI† for details). To confirm the suitability of this molecular target to our measurement approach, we initially performed gel analysis. First, we resuspended the raw material in a 1% SDS solution to denature and solubilize all proteins present. On gel, we observed a dominant band at the expected 22 kDa size for α-zein (Fig. 3b, lane 2). Additional lighter bands could be attributed to other isoforms (*e.g.* γ-zein[38]) and some minor dimer formation. We next resuspended in pure water using the same methods. Under these conditions, we found by gel that no proteins were soluble (Fig. 3b, lane 3), confirming the hydrophobic nature of all components of the original zein isolate. Finally, we resuspended the material in two different azeotropic mixtures (90% and 60% ethanol (v/v)) before

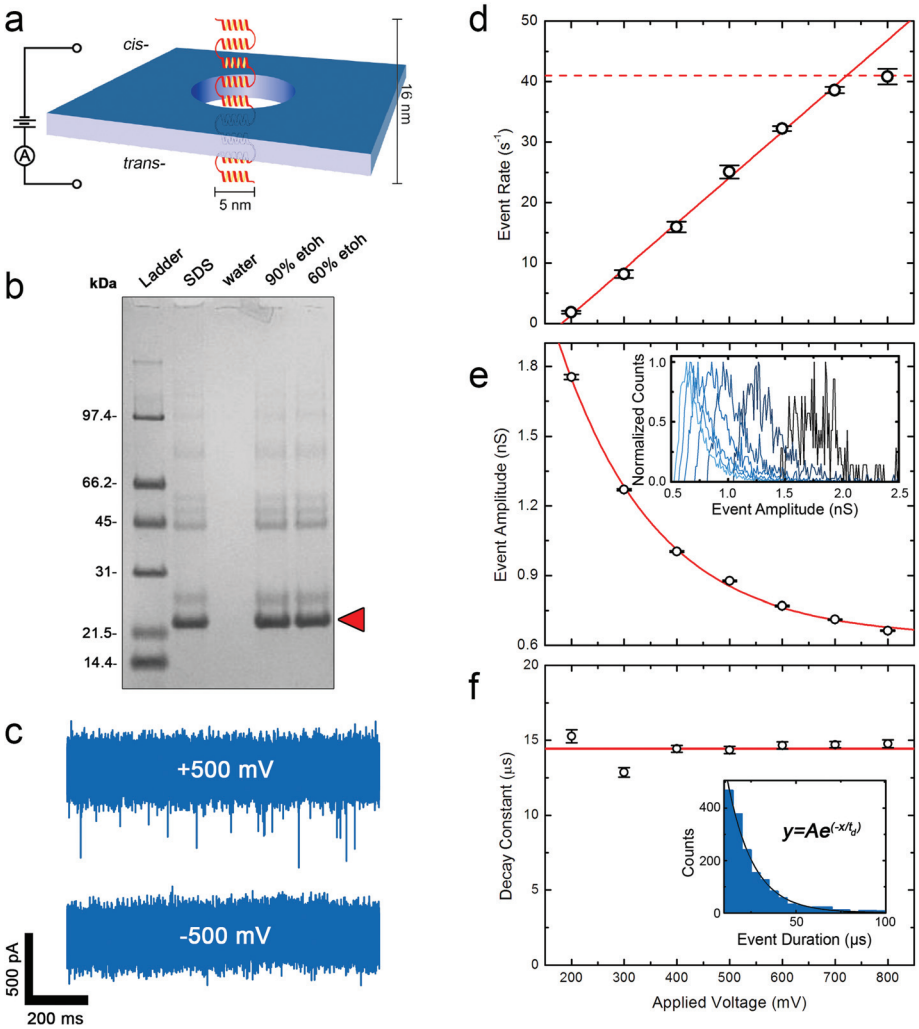

Fig. 3 (a) Cartoon of α-zein translocation through a SS-nanopore. Protein dimensions are indicated. (b) SDS-PAGE gel analysis of α-zein (22 kDa, red arrow) resuspended in SDS (lane 2), pure water (lane 3), 90% ethanol (lane 4), and 60% ethanol (lane 5). The protein is only insoluble in water. (c) Typical SS-nanopore current traces (in 3 M LiCl and 60% (v/v) ethanol, pore diameter 9 nm) with α-zein introduced to *cis*- chamber and either positive or negative voltage (500 mV) applied to the *trans*- chamber. Translocation events are observed only toward positive polarity. (d) Event rate for 10 μM α-zein as a function of applied voltage, showing linear dependence and eventual saturation. Solid line is a linear fit up to 700 mV and dashed line is approximate saturation rate. Each data point represents rate measured from a 150 s uninterrupted trace. (e) Mean event amplitude (depth) as a function of applied voltage. The individual data points represent the center of a Gaussian fit to an amplitude histogram and error bars are standard deviations. The red line is an exponential fit to the data. Inset: normalized event amplitude histograms from 200–800 mV (right to left). (f) Exponential decay constants derived from fits to event duration histograms as a function of applied voltage. No voltage dependence is observed. Inset: example event duration histogram (400 mV) and fit. For (e) and (f), from 200–800 mV, n = 190, 1008, 1764, 3225, 3823, 5172, and 5027, respectively.

Published on 27 April 2017. Downloaded by Wake Forest University on 20/06/2017 13:51:53.

running on denaturing gel. For each of these, a protein pattern emerged that was identical to that found in the SDS case (Fig. 3b, lanes 4 and 5), indicating that the protein isolate (predominantly α-zein) is indeed soluble under both ethanol concentrations. This result agreed well with previous reports of zeins in high ethanol solutions.[34]

Having established the alcohol solubility of our α-zein, we proceeded to perform SS-nanopore analysis on the material, using 3 M LiCl as an electrolyte to maximize signal-to-noise ratio. In an effort to minimize evaporation as a variable, and because α-zein solubility at 60% (v/v) ethanol is indistinguishable from that at a 90% (*cf.* Fig. 3b), we chose to use the lower alcohol concentration in our measurements. Fig. 3c shows example ionic current traces collected on a typical nanopore at both positive and negative polarity. The charge of α-zein is slightly negative,[39] but is not well characterized in ethanol/water mixtures, and so the direction of translocation could not be easily predicted *a priori*. Our measurement yielded events exclusively with positive voltage applied to the *trans* chamber, indicating that the net electrical force[17] was toward a positive bias. We also note that significant events were observed only with high protein concentration; indeed, measurements typically required concentrations in at least the μM range. This is about an order of magnitude higher than previous SS-nanopore studies of protein translocation in conventional fluids[17,40] and may suggest that either (i) a small driving force acts on α-zein under our conditions; (ii) that delivery of proteins to the pore mouth is reduced by altered diffusive kinetics in ethanol azeotropes; and/or (iii) that the majority of translocations are undetectable, as has been reported for hydrophyllic proteins in aqueous conditions.[41]

To explore this measurement further, we analyzed translocation event characteristics. We first noted that the event rate varied linearly with applied voltage up to a point, after which it saturated (Fig. 3d). This was in qualitative agreement with previous reports[40] and consistent with drift-dominated translocation dynamics. Examining event amplitude, we observed single, defined populations of mean depth over a large range of investigated voltage (200–800 mV, Fig. 3e, inset). Significantly, as applied voltage was increased, the measured histograms shifted towards smaller depths. This reduction was found to follow an exponential trend (Fig. 3e) and was generally suggestive of event chopping, driven by short translocation times.[41] Indeed, analysis of event dwell times showed small duration events with exponential distributions (ESI Fig. S4† and Fig. 3f, inset). We note that the majority of the observed events are less than the 33 μs duration below which distortions would be expected[41] for our filter conditions (20 kHz). Consequently, the resulting decay constants represent maxima rather than quantitative duration values. But, importantly, the distributions did not vary with applied voltage (Fig. 3f), further suggesting that the detected events represent only the slowest translocations as described above. This is likely enabled by strong stochastic interactions between the α-zein and the pore walls and indicates that temporal resolution still plays an important role, as it does in more conventional solvents.[41] Nevertheless, these results clearly demonstrate for the first time an ability to detect alcohol-soluble molecules using SS-nanopores.

Conclusion

In conclusion, we have reported on resistive-pulse sensing in azeotropic ethanol/water mixtures using SS-nanopores, accomplished by taking advantage of the intrinsic alcohol solubility of LiCl as an electrolyte. We first characterized LiCl ionic flux through individual nanopores over the full range of ethanol content, determining its dependence on both salt concentrations and pore diameter. We observed trends in conductance related to each of these factors that could be understood using established models with simple adjustments. We next used the system to measure α-zein, a model protein with solubility only in high-concentration alcohol solutions. Analysis of electrical translocations indicated only the slowest translocations could be resolved, similar to results in traditional solvents.[41] High bandwidth measurements would provide improved resolution, as they have elsewhere,[40] but detection of a molecular target that could not be probed in a conventional platform was clearly demonstrated. This work will enable SS-nanopores to be employed in measuring a host of traditionally challenging alcohol-soluble proteins,[1,2,42] and can be expanded further to probe alcohol-soluble synthetic nanoparticles[6–8] as well. This will create a powerful complement or alternative to existing analytical techniques like dynamic light scattering and electron microscopy.

Acknowledgements

We thank Prairie Gold, Inc. for the kind gift of Amazein™ raw zein protein for study. We also thank S. Harvey for help in performing the protein gels and O. K. Zahid for contributions to study preparation and useful discussions.

References

1 M. Pine, *J. Bacteriol.*, 1963, **85**, 301–305.
2 J. Mosse, *Fed. Proc.*, 1966, **25**, 1663–1669.
3 O. Molberg, S. N. Mcadam, R. Korner, H. Quarsten, C. Kristiansen, L. Madsen, L. Fugger, H. Scott, O. Noren, P. Roepstorff, K. E. A. Lundin, H. Sjostrom and L. M. Sollid, *Nat. Med.*, 1998, **4**, 713–717.
4 A. M. Klibanov, *Nature*, 2001, **409**, 241–246.
5 L. E. Bromberg and A. M. Klibanov, *Proc. Natl. Acad. Sci. U. S. A.*, 1995, **92**, 1262–1266.
6 E. A. Meulenkamp, *J. Phys. Chem. B*, 1998, **102**, 5566–5572.
7 N. Pinna, S. Grancharov, P. Beato, P. Bonville, M. Antonietti and M. Niederberger, *Chem. Mater.*, 2005, **17**, 3044–3049.
8 Y. Li, S. Liu, T. Yao, Z. Sun, Z. Jiang, Y. Huang, H. Cheng, Y. Huang, Y. Jiang, Z. Xie, G. Pan, W. Yan and S. Wei, *Dalton Trans.*, 2012, **41**, 11725–11730.

 This journal is © The Royal Society of Chemistry 2017

Published on 27 April 2017. Downloaded by Wake Forest University on 20/06/2017 13:51:53.

9 C. Dekker, *Nat. Nanotechnol.*, 2007, **2**, 209–215.
10 M. Wanunu, *Phys. Life Rev.*, 2012, **9**, 125–158.
11 J. L. Li, M. Gershow, D. Stein, E. Brandin and J. A. Golovchenko, *Nat. Mater.*, 2003, **2**, 611–615.
12 A. J. Storm, J. H. Chen, H. W. Zandbergen and C. Dekker, *Phys. Rev. E*, 2005, **71**, 051903.
13 G. M. Skinner, M. van den Hout, O. Broekmans, C. Dekker and N. H. Dekker, *Nano Lett.*, 2009, **9**, 2953–2960.
14 M. van den Hout, G. M. Skinner, S. Klijnhout, V. Krudde and N. H. Dekker, *Small*, 2011, **7**, 2217–2224.
15 D. Fologea, B. Ledden, D. S. McNabb and J. Li, *Appl. Phys. Lett.*, 2007, **91**, 053901.
16 D. S. Talaga and J. Li, *J. Am. Chem. Soc.*, 2009, **131**, 9287–9297.
17 M. Firnkes, D. Pedone, J. Knezevic, M. Doeblinger and U. Rant, *Nano Lett.*, 2010, **10**, 2162–2167.
18 A. S. Prabhu, T. Z. N. Jubery, K. J. Freedman, R. Mulero, P. Dutta and M. J. Kim, *J. Phys.: Condens. Matter*, 2010, **22**, 454107.
19 L. Bacri, A. G. Oukhaled, B. Schiedt, G. Patriarche, E. Bourhis, J. Gierak, J. Pelta and L. Auvray, *J. Phys. Chem. B*, 2011, **115**, 2890–2898.
20 A. R. Hall, J. M. Keegstra, M. C. Duch, M. C. Hersam and C. Dekker, *Nano Lett.*, 2011, **11**, 2446–2450.
21 E. A. Heins, Z. S. Siwy, L. A. Baker and C. R. Martin, *Nano Lett.*, 2005, **5**, 1824–1829.
22 D. Fologea, J. Uplinger, B. Thomas, D. S. McNabb and J. L. Li, *Nano Lett.*, 2005, **5**, 1734–1737.
23 S. J. Lee, J. Y. Kang, W. Choi and R. Kwak, *Small*, 2016, **13**, 1601725.
24 J. Feng, K. Liu, R. D. Bulushev, S. Khlybov, D. Dumcenco, A. Kis and A. Radenovic, *Nat. Nanotechnol.*, 2015, **10**, 1070–1076.
25 H. Mehdi, K. Binnemans, K. V. Hecke, L. V. Meervelt and P. Nockemann, *Chem. Commun.*, 2010, **46**, 234–236.
26 M. Li, D. Constantinescu, L. Wang, A. Mohs and J. Gmehling, *Ind. Eng. Chem. Res.*, 2010, **49**, 4981–4988.
27 R. M. M. Smeets, U. F. Keyser, D. Krapf, M. Y. Wu, N. H. Dekker and C. Dekker, *Nano Lett.*, 2006, **6**, 89–95.
28 W. M. Haynes, *CRC Handbook of Chemistry and Physics*, CRC Press, Boca Raton, FL, web version, 97th edn, 2016.
29 S. W. Kowalczyk, A. Y. Grosberg, Y. Rabin and C. Dekker, *Nanotechnology*, 2011, **22**, 315101.
30 M. Wanunu, T. Dadosh, V. Ray, J. Jin, L. McReynolds and M. Drndic, *Nat. Nanotechnol.*, 2010, **5**, 807–814.
31 F. H. J. van der Heyden, D. Stein and C. Dekker, *Phys. Rev. Lett.*, 2005, **95**, 116104.
32 C. Wohlfarth, in *Supplement to IV/6*, ed. M. D. Lechner, Springer, Berlin, Heidelberg, 2008, pp. 520–523.
33 A. Dill and O. Popovych, *J. Chem. Eng. Data*, 1969, **14**, 156–160.
34 T. J. Anderson and B. P. Lamsal, *Cereal Chem. J.*, 2011, **88**, 159–173.
35 Y. Luo and Q. Wang, *J. Appl. Polym. Sci.*, 2014, **131**, 40696.
36 J. P. Ortiz-Sánchez, F. Cabrera-Chávez and A. M. C. de la Barca, *Nutrients*, 2013, **5**, 4174–4183.
37 N. Matsushima, G. Danno, H. Takezawa and Y. Izumi, *Biochim. Biophys. Acta, Protein Struct. Mol. Enzymol.*, 1997, **1339**, 14–22.
38 A. Esen, *J. Cereal Sci.*, 1987, **5**, 117–128.
39 V. Cabra, R. Arreguin, A. Galvez, M. Quirasco, R. Vazquez-Duhalt and A. Farres, *J. Agric. Food Chem.*, 2005, **53**, 725–729.
40 J. Larkin, R. Y. Henley, M. Muthukumar, J. K. Rosenstein and M. Wanunu, *Biophys. J.*, 2014, **106**, 696–704.
41 C. Plesa, S. W. Kowalczyk, R. Zinsmeester, A. Y. Grosberg, Y. Rabin and C. Dekker, *Nano Lett.*, 2013, **13**, 658–663.
42 H. Yoshikawa, A. Hirano, T. Arakawa and K. Shiraki, *Int. J. Biol. Macromol.*, 2012, **50**, 1286–1291.